Digital Biomarkers

Health Measure – Research Article

Digit Biomark 2024;8:59–74
DOI: 10.1159/000538486

Received: September 25, 2023
Accepted: March 10, 2024
Published online: April 22, 2024

Feature Importance Analysis and Machine Learning for Alzheimer's Disease Early Detection: Feature Fusion of the Hippocampus, Entorhinal Cortex, and Standardized Uptake Value Ratio

Aya Hassouneh[a] Bradley Bazuin[a] Alessander Danna-dos-Santos[b]
Ilgin Acar[c] Ikhlas Abdel-Qader[a]
The Alzheimer's Disease Neuroimaging Initiative

[a]Electrical and Computer Engineering, Western Michigan University, Kalamazoo, MI, USA; [b]Department of Physical Therapy, Western Michigan University, Kalamazoo, MI, USA; [c]Department of Industrial and Entrepreneurial Engineering and Engineering Management, Western Michigan University, Kalamazoo, MI, USA

Keywords
Feature importance analysis and Alzheimer's disease · Alzheimer's disease early detection · Mild cognitive impairment conversion and mild cognitive impairment stable · Mild cognitive impairment conversion early detection

Abstract
Introduction: Alzheimer's disease (AD) is a progressive neurological disorder characterized by mild memory loss and ranks as a leading cause of mortality in the USA, accounting for approximately 120,000 deaths per year. It is also the primary form of dementia. Early detection is critical for timely intervention as the neurodegenerative process often starts 15–20 years before cognitive symptoms manifest. This study focuses on determining feature importance in AD classification using fused texture features from 3D magnetic resonance imaging hippocampal and entorhinal cortex and standardized uptake value ratio (SUVR) derived from positron emission tomography (PET) images. ***Methods:*** To achieve this objective, we employed four distinct classifiers (Linear Support Vector Classification, Linear Discriminant Analysis, Logistic Regression, and Logistic Regression Classifier with Stochastic Gradient Descent Learning). These classifiers were used to derive both average and top-ranked importance scores for each feature based on their outputs. Our framework is designed to distinguish between two classes, AD-negative (or mild cognitive impairment stable [MCIs]) and AD-positive (or MCI conversion [MCIc]), using a probabilistic neural network classifier and the Alzheimer's Disease Neuroimaging Initiative (ADNI) database. ***Results:*** The findings from the feature importance highlight the crucial role of the GLCM texture features extracted from the

Data used in the preparation of this article were obtained from the Alzheimer's Disease Neuroimaging Initiative (ADNI) database (adni.loni.usc.edu). As such, the investigators within ADNI contributed to the design and implementation of ADNI and/or provided data but did not participate in the analysis or writing of this report. A complete listing of ADNI investigators can be found at http://adni.loni.usc.edu/wpcontent/uploads/how_to_apply/ADNI_Acknowledgement_List.pdf.

karger@karger.com
www.karger.com/dib

Correspondence to:
Aya Hassouneh, aia.hassouneh@gmail.com

hippocampus and entorhinal cortex, demonstrating their superior performance compared to the volume and SUVR. GLCM texture AD classification achieved approximately 90% sensitivity in identifying MCIc cases while maintaining low false positives (below 30%) when fused with other features. Moreover, the receiver operating characteristic curves validate the GLCMs' superior performance in distinguishing between MCIs and MCIc. Additionally, fusing different types of features improved classification performance compared to relying solely on any single feature category. ***Conclusion:*** Our study emphasizes the pivotal role of GLCM texture features in early Alzheimer's detection.

Introduction

Alzheimer's disease (AD) is a progressive degenerative neurological condition that causes damage to the brain [1]. Its clinical onset is marked by mild memory lapses and mild cognitive impairments (MCI) resulting from focal damage to the hippocampal and entorhinal cortical areas [1]. With progression, severe memory loss arises, and other cortical areas become compromised, resulting in non-cognitive symptoms [1]. Currently, no clinical or surgical interventions are available to reverse its effects, but a pressing need exists to improve its early diagnosis. An early diagnosis becomes crucial for the initiation of early-on personalized care and, thus, improvement in quality of life as AD progresses [2, 3]. With the constant improvement in image quality and clinical procedures, imaging has become a suitable non-invasive tool for the early diagnosis of degenerative processes, especially when knowledge extracted from multiple modalities can be combined in the fused model for enhanced feature classification.

Previous studies have investigated the potential and benefits of combining multiple modalities for the early detection of AD. For example, Wang et al. [4] used the partial least squares (PLS) method to distinguish between people with MCI who will develop AD and those who will not, using a variety of imaging techniques, including magnetic resonance imaging (MRI), 18F-fluorodeoxyglucose positron emission tomography (FDG-PET), and 18F-florbetapir-PET. Two PLS models were used: informed and agnostic. The informed PLS model that used all three modalities had better classification accuracy, sensitivity, and specificity than the single-modality model. Similarly, Zhang et al. [5] used a multimodal approach that combined MRI, functional (fMRI), and PET features to classify AD, MCI, and healthy controls. Gupta et al. [6] also concentrated on fusing data from structural, diffusion, and functional neuroimaging with multimodal properties derived from APOE genotype information to increase the accuracy and knowledge of AD.

This study focused on using two imaging modalities: MRI and PET. Our rationale is based on the premise that feature extraction from multiple modalities can enhance the ability to capture subtle abnormalities in the neural substrate caused by the degenerative process and increase the reliability of the diagnosis at the onset and in its early stages. Here, we focused on MRI and PET images captured from the hippocampus and entorhinal cortices of patients diagnosed with MCI. Our choice for these modalities is based on the fact that both MRI and PET are currently used independently to track changes in cortical substrate and to diagnose AD. These modalities can clearly distinguish between different soft tissues, have non-invasive qualities, and have detailed imagery [7, 8]. MRI images can be taken from three main directions: sagittal, coronal, and axial views. Coronal views of the structural MRI images can be segmented to assess the differences between MCIs resulting from either AD or other pathologies.

Recently, the field of biomarkers in AD has witnessed a transformative shift toward digital biomarkers [9]. AD biomarkers are derived from various sources, such as the traditional sources of measurements taken from cerebrospinal fluid (CSF) analysis and neuroimaging techniques taken from various imaging modalities. However, digital biomarkers, such as speech characteristics, offer non-invasive monitoring and detection of AD. Digital biomarkers have the potential for continual, non-invasive monitoring, potentially enabling early detection and longitudinal tracking of cognitive decline [10]. While we focus on using measurements taken from imaging modalities due to the wealth of the available datasets and their high accuracy, we do so without overshadowing the emerging importance of recent digital biomarkers. We believe that integrating both has the potential to present an exhaustive model of AD progression, overcome single biomarker limitations, and allow for early detection, intervention, and personalized prognosis.

Our focus on the hippocampus and entorhinal cortex regions is based on the premise that these brain regions are often among the first to show signs of degenerative damage [11, 12]. The hippocampus and entorhinal cortex have fusion features that can be exploited to identify AD early warning symptoms. Brain MRI scans can be used to extract these features. For instance, the hippocampus and

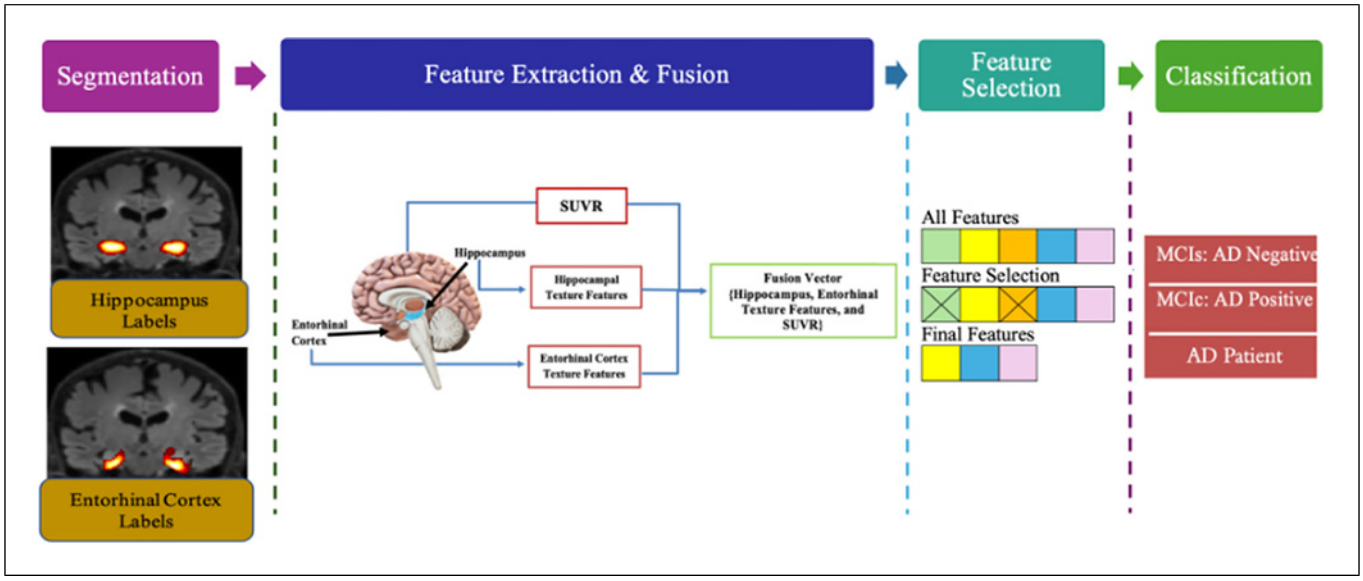

Fig. 1. System process block diagram. It shows the four main processes of the proposed framework: segmentation, feature extraction and fusion, feature selection, and stage prediction.

entorhinal cortex can be used to extract structural features from MRIs like volume and 2D-GLCM [13–16]. In addition, these techniques can be used to recognize the presence of higher-than-normal concentrations of amyloid-β (Aβ) peptide and Tau [17]. The accumulation of Aβ and Tau-PET (Aβ and Tau-PET) is now recognized to be significantly higher in MCI patients who developed AD within 2 years compared to those who did not [18]. Therefore, the purpose of this study is to assess the significance and contributions of various features in the early prediction of AD. This involves using fused texture features extracted from 3DMRI images of the hippocampal and entorhinal cortex, along with the standardized uptake value ratio (SUVR) derived from PET images. The verification of the feature importance analysis findings is accomplished using the probabilistic neural network (PNN) classifier within this research by differentiating between two primary classes: (1) individuals with stable MCI (MCIs AD-negative) and (2) those progressing to AD (MCIc AD-positive). This exploration not only emphasizes the importance of specific brain regions but also underscores the significance of texture-based features in the early detection of AD and its progression.

Methodology

To achieve our goals, we developed a framework that calculates feature importance using fused texture features to optimize classification accuracy. The proposed framework has four main processes: segmentation, feature extraction and fusion, feature selection, and classification. These processes are shown in the system process block diagram in Figure 1 (shown in Fig. 1).

Segmentation of Alzheimer's Disease Neuroimaging Initiative Dataset

Data Acquisition – Alzheimer's Disease Neuroimaging Initiative Dataset

For the success of our project, data from the Alzheimer's Disease Neuroimaging Initiative (ADNI) database were used (www.loni.ucla.edu/ADNI). The ADNI was established in 2003 by the National Institute on Aging (NIA), the National Institute of Biomedical Imaging and Bioengineering (NIBIB), the Food and Drug Administration (FDA), private pharmaceutical companies, and non-profit organizations. The main objective of the ADNI has been to determine whether serial MRI, PET, other biological markers, clinical evaluation, and neuropsychological testing may be integrated to track the evolution of MCI and lead to early AD detection [19].

This study involved randomly downloading the coronal MRIs of 137 participants from the ADNI database and categorizing them into two groups: MCIc and MCIs. The number of MRIs for each group is roughly the same, so the results of the analysis are not biased.

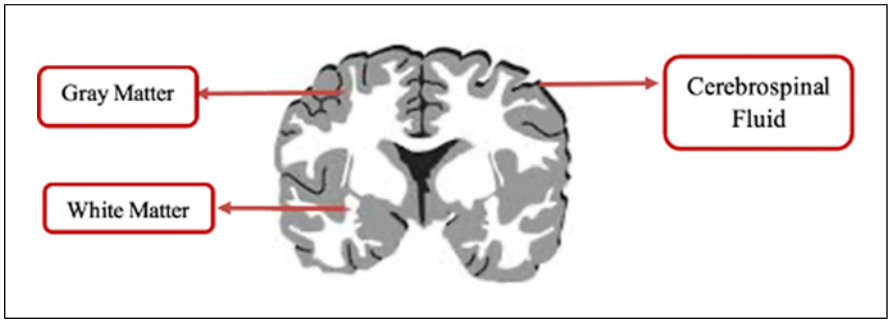

Fig. 2. Segment of the brain highlighting several regions of interest including CSF and white and gray matters.

Achieving a balance in the dataset resulted in a more accurate depiction of the variations between the groups and the robustness of the results by avoiding sampling bias.

FMRIB Software Library for Hippocampus and Entorhinal Cortex Segmentation

FMRIB Software Library – FMRIB's Integrated Registration and Segmentation Tool (FSL-FIRST) is one of the most frequently used segmentation techniques and is widely used in the neuroimaging research community [20]. It is a tool that is automated to use flexible models to divide brain images into different segments. It was developed by the FMRIB group at Oxford University and uses a Bayesian approach to segment and register subcortical brain structures using shape and appearance models. Thus, it is a part of the FSL, which is a collection of image analysis tools specifically designed for fMRI data. It can segment several brain components, including gray matter, white matter, and CSF (as shown in Fig. 2), and it reliably aligns brain images using a mix of intensity-based and surface-based registration techniques [20].

The CSF surrounds the brain and spinal cord, providing essential nourishment and acting as a protective cushion [22]. The white matter consists of bundles of nerve fibers that facilitate communication between different brain regions [23], while the gray matter encompasses the cell bodies of neurons and serves as the primary site for information processing and integration [24]. As the hippocampus and entorhinal cortex are two of the brain regions that are most severely affected by the disease and are often among the first to show signs of damage [11, 12], the software FSL-FIRST was used to identify and segment them from the MRI images (shown in Fig. 2).

MRI images can be taken from three main directions: sagittal, coronal, and axial views. Coronal views of the structural MRI images were segmented to assess the differences between MCIs (AD−ve) and MCIc (AD+ve). As on coronal views, the hippocampus and entorhinal cortex can be easily identified [21, 22]. The differences are visible between MCIs (−ve AD), MCIc (+ve AD), and AD, on a coronal view, with our region of interests pointed by arrows, as shown in Figure 3 (shown in Fig. 3).

The process of segmenting the hippocampus and entorhinal cortex into distinct regions involves several steps. These steps include preparing the data, using FSL's segmentation tools to identify the structures, and creating masks to isolate them, detailed in the following instructions:

a. Brain Extraction Tool (BET) is used to extract the brain from the skull-stripped T1-weighted images. In other words, it was used to remove non-brain tissue and improve image quality [23, 24].
b. Standard brain: T1 images must be aligned with a standard brain. Stand-alone registration can be carried out by first using linear registration, FMRIB's Linear Image Registration Tool (FLIRT), and then non-linear registration (FNIRT). To align structural images with a standard, FLIRT can be used to register the MRI T1-weighted images to a common space and thus create a template of the hippocampus and entorhinal cortex, aligning the MRI T1 images with the standard space (MNI152_T1_2 mm) [23, 24].
c. Atlas-based segmentation: the template and atlases (Harvard-Oxford subcortical structural atlas and Juelich Histological Atlas) were used to segment the hippocampus and entorhinal cortex in each individual aligned T1-weighted image [23, 24].
d. Mask creation: binary masks for the hippocampus and entorhinal cortex were created using the segmentation results [23, 24].
e. Visual inspection: FSL's visualization tool (FSLeyes) was used to inspect the segmentation results and check if the segments are consistent with the underlying anatomy [23, 24].

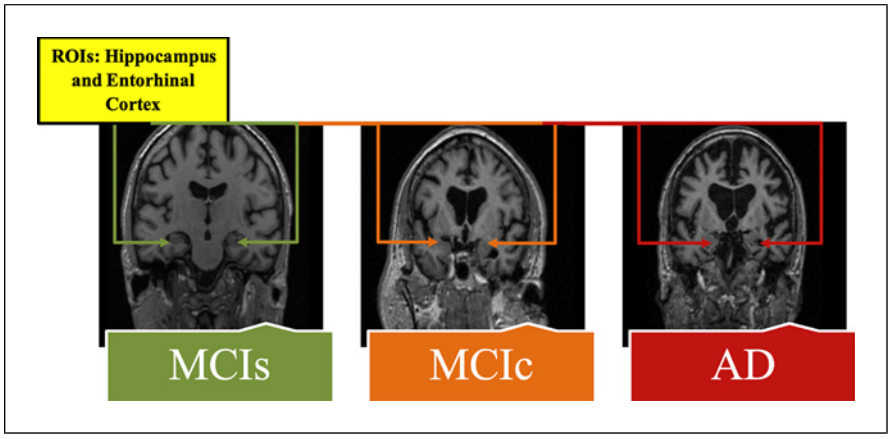

Fig. 3. Differences between MCIs (−ve AD), MCIc (+ve AD), and AD [27]. MCIs is the class of patients who have stable MCI and will not convert into AD in the future, MCIc is the class of those patients who will convert from MCI to AD diagnosis (i.e., positive prediction), and finally, AD patients.

f. Orientation check: this was done by loading the left and right hippocampus and entorhinal cortex masks and checking their orientation with the orientation of each MRI scan. If the orientations were not the same, the masks were transformed to match the orientation of the MRI scan. The MRI data were then extracted based on the mask, resulting in a Neuroimaging Informatics Technology Initiative (NIFTI) image containing only the regions of interest (ROIs).

Feature Extraction

In this study, texture features (2D-GLCM and volume) were extracted from the hippocampus and entorhinal cortex in ADNI MRIs due to their significance in diagnosis [25–28]. Additionally, since the buildup of Aβ and Tau can serve as a biomarker for the early diagnosis of AD [18, 29], the accumulation of proteins Aβ and Tau abnormalities was measured using the SUVR from the extracted hippocampus and entorhinal cortex.

Hippocampal and Entorhinal Cortex 2D-GLCM Texture Features

Textural feature extraction is achieved using 2D-GLCM. GLCM provides a relative assessment of the characteristics of two or more pixel values that occur at a particular point. Each element of the matrix Pij represents the number of times the pair of adjoining pixels with pixel values i and j occur in the image. A case of a 2D image is computed using a displacement vector d and orientation θ. Construction of GLCM is determined by the radius, angle, and quantized gray levels. Changing these parameters has a significant influence on the computation of GLCM and classification.

Radius Choice

The radius (offset) in GLCM refers to the distance in various directions between the pixel under consideration and the adjoining pixel and is normally between 1 and 10, but it may be greater depending on the image being processed. Smaller radii are frequently preferred because the probability of identifying two pixels with comparable gray levels improves when pixels are closer together, thus decreasing the distance yields better results than increasing the distance [30]. In the context of this research, we chose a smaller radius, denoted by d = 1, 3, 5. This option allows us to detect differences in intensity between pixels that may indicate the presence of pathological disorders.

Angle Choice

Different angles can provide different GLCMs. As shown in Figure 4, each pixel of interest has eight neighboring pixels, so we can have 8 GLCMs with each neighbor; however, choosing 0 and 180 provides identical GLCMs based on the GLCM definition. So, for a 2D image, there will be four GLCM captured at angles of 0, 45, 90, and 135 degrees [30] (shown in Fig. 4).

Gray-Level Choice

The number of gray levels determines the size of GLCM. For example, if we examine 256 gray levels, the final GLCM will be 256 × 256 = 65,536 in size. If the image contains multiple gray levels, using a higher gray level for GLCM calculation will improve classification accuracy. Using all the matrix entries in the feature vector will considerably expand its length. This number can be reduced by extracting some matrix properties such as dissimilarity, correlation, homogeneity, contrast, and angular second moment (ASM) [30].

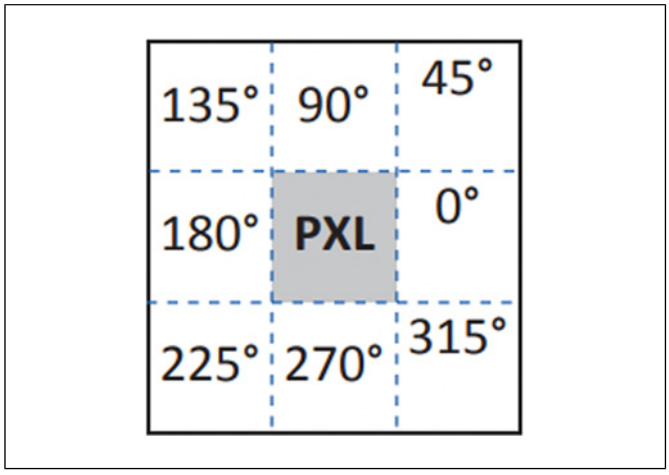

Fig. 4. Values of θ between the center pixel and its eight neighboring pixels [36].

Finding the 2D-GLCM matrix for each 3D hippocampus and entorhinal cortex required the following processes to take place:

a. Calculating the GLCM matrix: for each 2D slice, calculate the GLCM using a combination of offsets d ∈ {1, 3, 5} and orientations θ ∈ {0°, 45°, 90°, 135°}. This gives a 2D-GLCM matrix for each slice. It should be observed that {180°, 225°, and 270°} were left out to prevent repetition.
b. Combining the GLCM matrices: create a single 2D-GLCM matrix for the entire hippocampus and entorhinal cortex by combining the 2D-GLCM matrices for all slices of each ROI along each of the three orthogonal axes.
c. Analyzing the GLCM matrix: use statistical measures such as homogeneity, contrast, and correlation to analyze the texture features of the hippocampus and entorhinal cortex and extract relevant information based on the outright inconsistencies between couples of gray levels or mean 2D-GLCM levels. Gray-level values represent the brightness or intensity levels of pixels in an image [31, 32].

The following textural details are among the textural characteristics of interest [31, 32]. We define key variables as follows: N is the number of gray levels in the ROI, and N × N is the size of the normalized 2D-GLCM. P_{ij} is the number of occurrences of gray levels *iandj* given a certain (d,θ) pair, μ is the mean, and σ is the standard deviation within the ROI.

A. Contrast. The contrast value measures the spatial variations or differences in pixel intensity within an ROI and is computed using Equation 1:

$$CON = \sum_{i,j=0}^{N-1} P_{ij}(i-j)^2 \quad (1)$$

B. Dissimilarity. It is used to assess the degree of divergence between two ROIs and is defined by Equation 2.

$$DISS = \sum_{i,j=0}^{N-1} P_{ij}\left|i-j\right| \quad (2)$$

C. Homogeneity. Homogeneity or inverse difference moment (IDM) is a measure of uniformity of the distribution of gray levels in the ROI around the diagonal, and is defined by Equation 3:

$$HOM = \sum_{i=0}^{N-1}\sum_{j=0}^{N-1} \frac{Pij}{1+(i-j)^2} \quad (3)$$

D. Correlation. The correlation feature calculates the linear dependence between a pixel and its neighbor throughout the entire ROI using Equation 4:

$$Corr = \sum_{i=0}^{N-1}\sum_{j=0}^{N-1} (Pij)\left[\frac{(i-\mu_i)(j-\mu_j)}{(\sigma_i)(\sigma_j)}\right] \quad (4)$$

where σ_i and σ_j are the standard deviations of the rows and columns of the GLCM, respectively.

E. ASM. It provides the GLCM's element squared sum, which is a measure of uniformity, and can be calculated using Equation 5:

$$ASM = \sum_{i=0}^{N-1}\sum_{j=0}^{N-1} (Pij)^2 \quad (5)$$

Feature Engineering: Creating a Single Texture Feature Using Histogram Techniques

Feature engineering is a critical step that aims to extract and create meaningful representations of the original features for machine learning tasks [33]. In this section, we demonstrated the histograms to extract a single feature from the entorhinal cortex and hippocampus texture features for classifying cognitive impairment. The histogram approach involves creating histograms for GLCM features to capture value distributions. Introducing histogram bins or counts as a new feature provides insights into the prevalence and strength of texture patterns. It is appropriate for situations in which the statistical distribution of GLCM features and the significance of texture pattern frequency or intensity are important, such as image classification tasks where texture patterns are discriminative variables [34]. As the distribution of values of the GLCM features is critical for our purpose and we want to capture the occurrence and strength

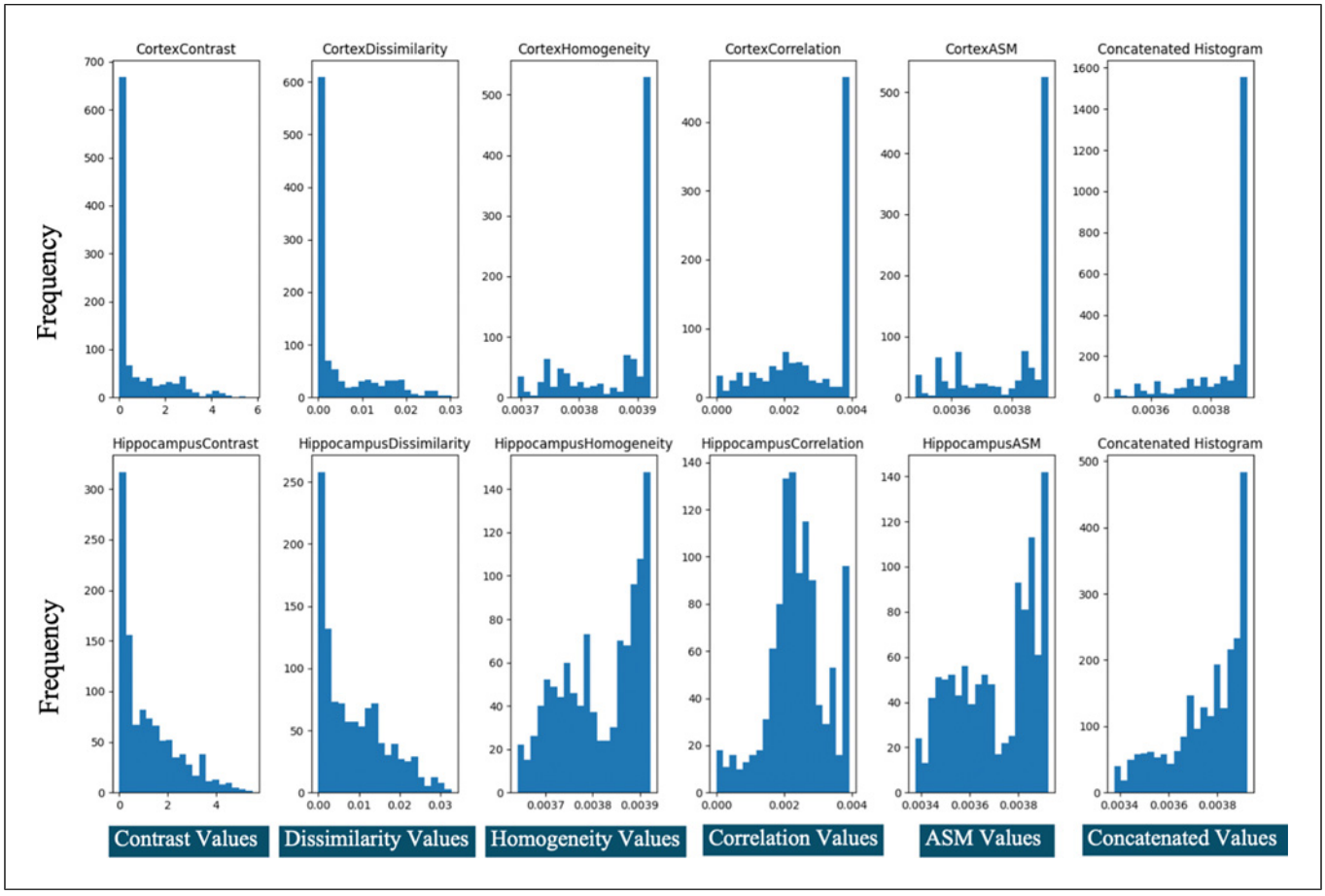

Fig. 5. Feature engineering: construction of histogram features for the entorhinal cortex and hippocampus.

of the texture patterns, the histogram is selected as the most effective for creating a new single texture feature from the major texture features.

Figure 5 illustrates the creation of individual histograms for each single feature extracted from both the entorhinal cortex and the hippocampus. These histograms are then concatenated, resulting in a single, comprehensive histogram feature for each region. By focusing on the distribution of values in the GLCM features and capturing the occurrence and strength of texture patterns, the histogram approach effectively generates a single texture feature that encapsulates the most relevant information from the original features (shown in Fig. 5).

Hippocampal and Entorhinal Cortex Volume Extraction

Several studies have shown that measuring the hippocampus and entorhinal cortex size is a useful method for identifying and monitoring a variety of brain disorders, including AD [13, 35–38]. Hence, using Equations 6 and 7, the total hippocampus and entorhinal cortex volumes in mm^3 for each participant were determined in cubic millimeters.

$$T_{HV} = L_{HV} + R_{HV} \tag{6}$$

where T_{HV} represents the total hippocampal volume, L_{HV} represents the left hippocampal volume, and R_{HV} represents the right hippocampal volume.

$$T_{ECV} = L_{ECV} + R_{ECV} \tag{7}$$

where T_{ECV} represents the total entorhinal cortex volume, L_{ECV} represents the left entorhinal cortex volume, and R_{ECV} represents the right entorhinal cortex volume.

The volume of each hippocampus and entorhinal cortex was determined by adding the non-zero volumes per voxel, using Equation 8 [39]:

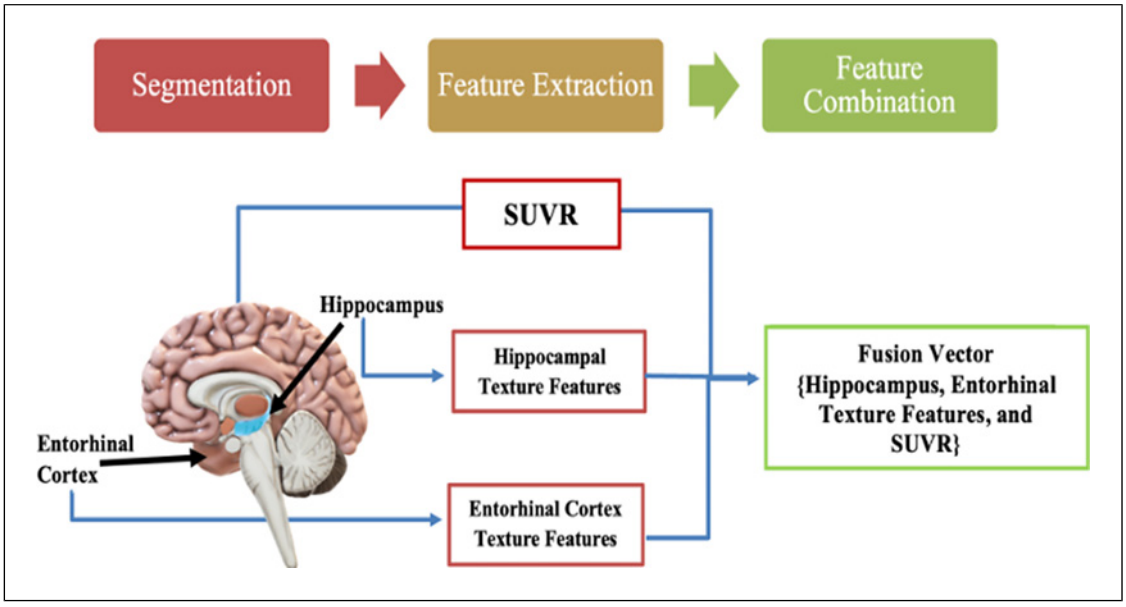

Fig. 6. Hippocampus, entorhinal cortex texture features, and SUVR extraction and fusion. The texture features include contrast, dissimilarity, homogeneity, ASM, correlation, and volume within these regions, combined with the measured SUVR.

$$Right\ ROI\ Volume = \sum_{k=0}^{n-1} voxel\_volume^{k};\ voxel\_volume > 0 \quad (8)$$

where n = number of voxels and voxel_volume = x-pixel-dimension * y-pixel-dimension * z-pixel-dimension.

SUVR – Amyloid (β) Peptide and Tau Abnormalities

The SUVR is a metric used to measure the accumulation of a radiotracer relative to a reference region in particular brain regions [40]. The average uptake of the radiotracer in a particular ROI (the hippocampus and entorhinal cortex) is divided by the average uptake in a reference region, such as the cerebellum. The cerebellum is often used as the reference region because it exhibits a relatively stable uptake across different individuals and situations. Equation 9 illustrates how to measure SUVR for the hippocampus.

$$SUVR = \frac{Average\ uptake\ in\ the\ hippocampus}{Average\ uptake\ in\ the\ cerebellum} \quad (9)$$

SUVR is a relative measurement and does not give an exact reading of the levels of amyloid or tau. However, it can be used to assess the amount of accumulation over time or compare the levels of these proteins in various people's brains, as well as to identify people with various stages of AD and other neurodegenerative diseases [41]. Thus, SUVR can be used to distinguish between MCIs and MCIc. A higher SUVR value indicates a higher level of tau or amyloid accumulation in the brain, which is associated with an increased risk of developing neurodegenerative diseases such as Alzheimer's [42].

Feature Fusion – Hippocampal, Entorhinal Cortex Texture Features, and SUVR

There is complementing information in the many biomarkers collected from various neuroimaging modalities [43–45]; therefore, feature fusion is pursued. Feature vectors are merged with the numerical features obtained from the ROI segments through concatenation. These fusion vectors are comprised of texture features of the hippocampus and entorhinal cortex from the segmented MRI images, as well as SUVR from the PET images, as illustrated in Figure 6. The resulting fusion vectors were then classified using benchmarked methods such as PNN classifiers (shown in Fig. 6).

Feature Importance Analysis

The classifiers used by [46] were used to find feature importance. These classifiers are selected for their ability to reveal feature importance and produce probability outputs. This determination of feature importance was primarily reliant on the assigned weights to the individual features. Furthermore, to calculate the overall feature

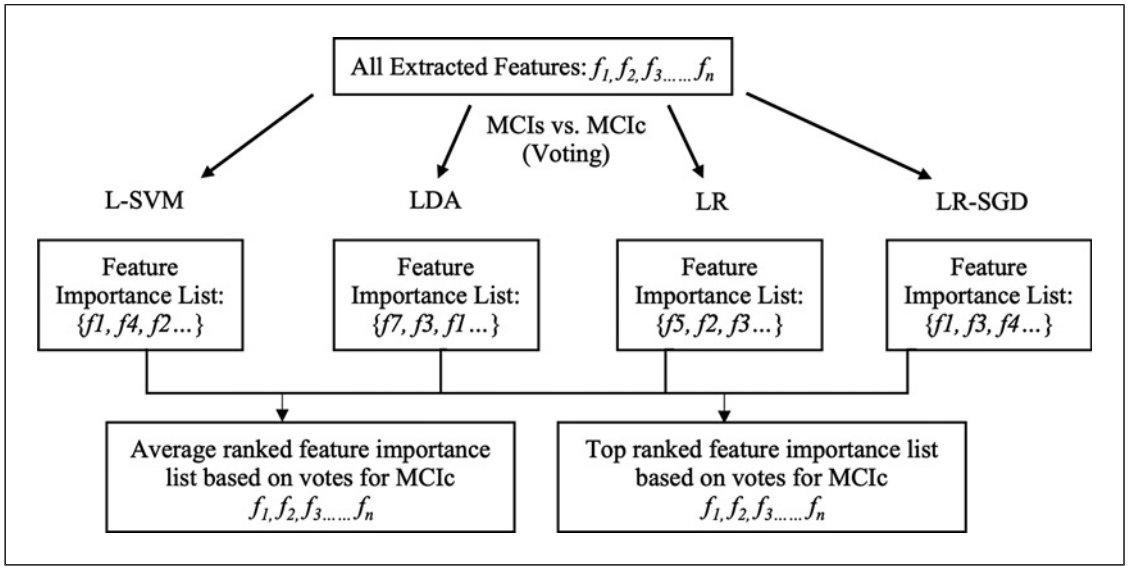

Fig. 7. Feature importance analysis using L-SVM, LDA, LR, and LRSGD.

importance, averaging and top-ranked approaches were adopted, considering the feature importance output from each classifier that contributed to the final decision through voting.

The following are the classifiers that were used to find feature importance:

a. Linear Support Vector Classification (L-SVM) [47]
b. Linear Discriminant Analysis (LDA) [48]
c. Logistic Regression (LR) [49]
d. Logistic Regression Classifier with Stochastic Gradient Descent Learning (LRSGD) [50]

The feature importance analysis involved combining four different classifiers: L-SVM, LDA, LR, and LRSGD Classifier, as shown in Figure 7. The average importance and the top-ranked importance of each feature were then calculated based on the output of these classifiers, providing valuable insights into the contribution of different features in classifying the output (shown in Fig. 7).

Classification Methods

The PNN model was selected to continue based on its strengths as a robust classification algorithm, its capacity to offer probability distributions across classes, and its established effectiveness in similar problem domains [51, 52]. PNN is a feed-forward neural network that combines Kernel-Fisher discriminant analysis and the Bayesian network [53]. PNN requires less retraining time and computational resources when new samples are added or removed compared to some other models since it uses lazy learning and saves parameters for predictions [53].

Experimental Work Design

In Figure 8, the experimental work design is presented. The extracted features of the hippocampus and entorhinal cortex are fused and saved in a CSV file. Those features are labeled by adding another column that contains the output features. The output labels are MCIs: AD−ve and MCIc: AD+ve. Then, both average and top-ranked techniques were used to determine the significance of each feature in the output. Finally, the PNN model was implemented using the fused features to test their strength in classifying MCIc individuals (shown in Fig. 8).

Results

After determining the 2D gray-level co-occurrence matrices, volume, and ratio of SUVR from both the hippocampus and entorhinal cortex, these matrices and ratios were combined at the feature level to form the feature fusion vectors.

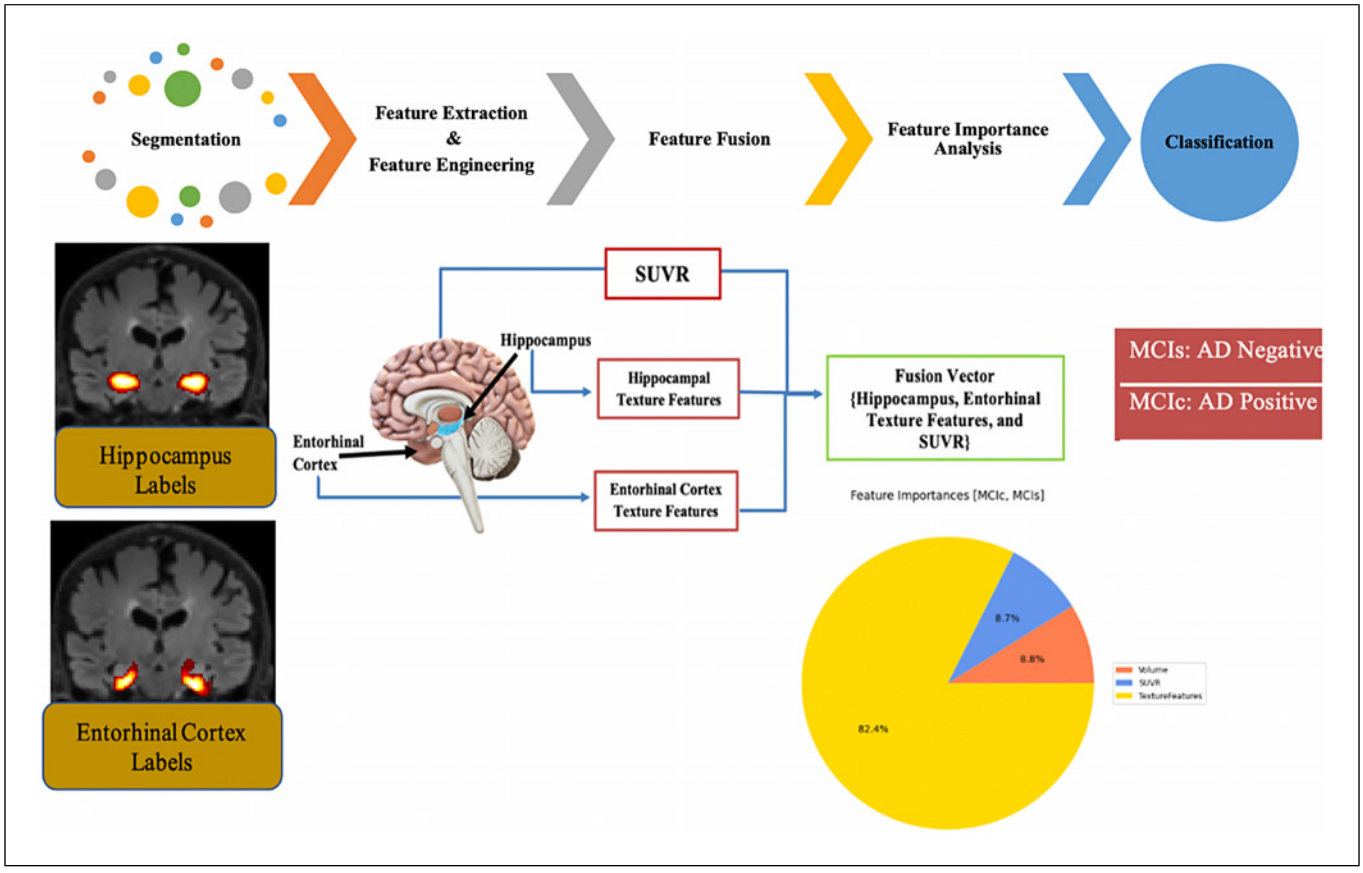

Fig. 8. Experimental work design.

Feature Importance Analysis – Highlighting the Significance of New Texture Features, Volumes, and SUVRs in the Hippocampus and Entorhinal Cortex

The approach for determining feature importance in this study was adapted from the work of [46]. Similar to their methodology, the feature importance analysis involved combining four different classifiers: L-SVM, LDA, LR, and LRSGD classifier. The feature importance analysis included the determination of the average importance and top-ranked importance for each feature, providing insights into the contribution of different features in classifying the output.

The feature importance visualization is presented using Figure 9, where each slice corresponds to a distinct feature category. The categories are as follows:

1. Volume: this category includes the hippocampus volume and cortex volume features.
2. SUVR: this category consists of the hippocampus SUVR and cortex SUVR.
3. Texture features: this category includes the newly engineered texture features obtained through feature engineering for both hippocampus texture features and cortex texture features (shown in Fig. 9).

Figure 9 clearly illustrates feature importance determined through the average and top-ranked methods. Both approaches illustrate that the texture features extracted from the entorhinal cortex and hippocampus outperformed the volume measurements of the cortex and the hippocampus, which were less important in the analysis. Additionally, the volume and SUVR exhibited the least significance in contributing to the output.

This finding is consistent with prior research conducted by [54, 55], where they demonstrated that texture features extracted from the hippocampus significantly outperformed the volume in terms of predictive accuracy for AD. Texture analysis (TA) has been successfully applied in previous research to produce imaging biomarkers for AD. They enable the identification of changes in MRI image pixel intensity caused by key characteristics of early-stage AD, such as neurofibrillary tangles and Aβ peptides, which are not directly detectable by human eyes [56].

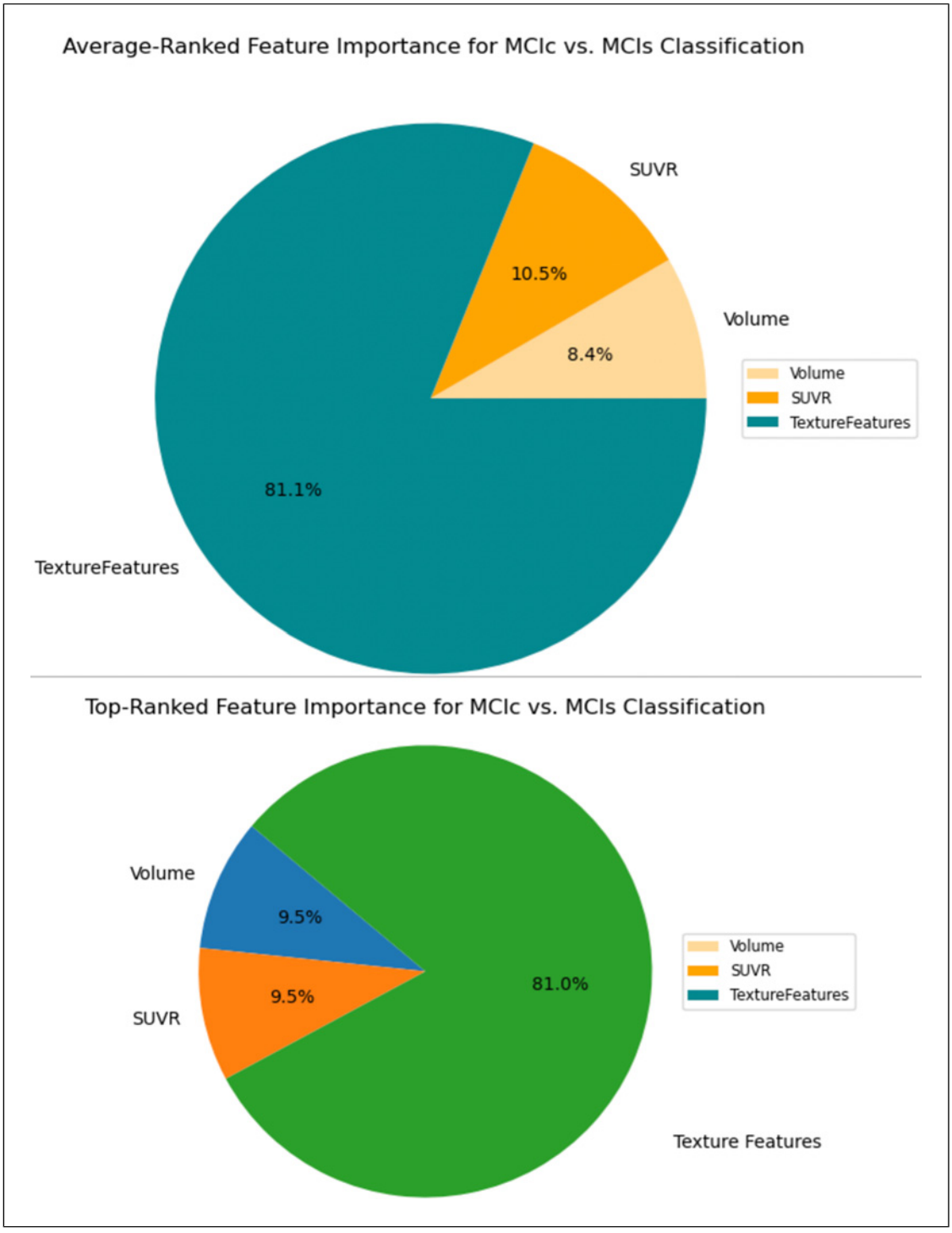

Fig. 9. Feature importance analysis using L-SVM, LDA, LR, and LRSGD classifiers.

Table 1. Performance factors (validation and test accuracy, precision, sensitivity, specificity, F1 score, and AUC) for all feature combinations using PNN algorithm for MCIs versus MCIc

Features	Validation accuracy	Test accuracy	Precision	Sensitivity	Specificity	F1 score	AUC
Volumes	55.56	80.0	83.3	83.3	83.3	80.0	83.0
GLCMs	90.3	91.44	91.9	92.3	92.3	91.4	92.0
SUVRs	70.0	50.0	50.0	49.5	49.5	48.6	50.0
Volumes + GLCMs	91.29	89.59	90.5	90.7	90.7	89.6	91.0
Volumes + SUVRs	45.45	66.67	43.0	50.0	50.0	40.0	50.0
GLCMs + SUVRs	90.9	88.67	90.1	89.6	89.6	88.7	90.0
All features	92.15	92.89	93.5	93.2	93.2	92.9	94.0

Impact of Hippocampal and Entorhinal Cortex 2D-GLCM, Volume, and SUVR on Early Detection of AD

The objective is to demonstrate the importance of different features found in the previous section by evaluating the accuracy of the various feature combinations using the PNN classifier for early diagnosis of AD in individuals with MCIs compared to those who will later develop AD (MCIc). As presented in Table 1, the PNN classifier used several fusions of features extracted from the hippocampus and entorhinal cortex, including GLCMs, volumes, and SUVRs. Each feature category represents a unique set of information derived from medical imaging data, and their significance in classifying AD development is of particular interest. Validation accuracy, test accuracy, precision, sensitivity (also known as recall or true-positive rate), specificity (true-negative rate), F1 score, and area under the receiver operating characteristic (AUC-ROC) curve were the metrics used for performance evaluation.

The performance of the PNN classifier using individual features was as follows: the model using just volumes achieved a decent accuracy of 80.0% on the test set but had difficulty distinguishing between MCIs and MCIc, as demonstrated by its relatively low sensitivity and F1 score. The GLCMs texture feature, on the other hand, performed very well, obtaining 91.44% accuracy on the test set with high sensitivity and specificity, indicating its strong ability to accurately classify MCIs and MCIc cases. In addition, the fusion of volumes and GLCM features performed well, with 89.59% accuracy on the test set and a high F1 score. Additionally, the fusion of GLCM and SUVR features exhibited excellent performance with 88.67% accuracy on the test set. However, the SUVR feature alone did not perform well on the test set, as indicated by its low accuracy, sensitivity, and specificity (50%, 49.5%, and 49.5%, respectively), suggesting a lack of discriminative power between the two classes. Fusion of Volumes and SUVRs performed poorly as well, with relatively low accuracy and F1 score (66.67% and 40%, respectively), struggling to correctly identify both MCIs and MCIc cases.

The most notable result was produced when the 2D-GLCM texture features were fused with all the features, resulting in the best performance. In this case, the model obtains a test set accuracy of 92.89% and displays a strong capacity to correctly classify both MCIs and MCIc instances, as evidenced by its high sensitivity, specificity, and F1 score.

While our study aligns with prior research [46] in recognizing the significant impact of texture features on the classification results, it distinguishes itself by focusing on the classification of "MCIs and MCIc," a different patient group than that of "healthy controls and AD" group explored in [46]. Our contribution to this work is also through feature the engineering technique, that is, standardizing all texture features for consistent analysis across various features (GLCM texture features, volume, and SUVR) for both the hippocampus and entorhinal cortex regions. These unique aspects of our research confirm and deepen the understanding of the significance of texture features in the classification of MCIs and MCIc patients, offering a more comprehensive perspective on their role in cognitive impairment. Furthermore, the study highlighted the significance of using several features in the classification of MCIs and MCIc patients. The fusion of volumes, GLCMs, and SUVRs yields positive results.

To summarize the results presented previously, we used Figure 10 which displays the chart of validation accuracy and test accuracy to allow for a comparison of feature performance for early AD detection. It includes volumes, GLCMs, SUVRs, and their various combinations. It highlights the importance of GLCM texture features as significant biomarkers for the early detection of AD. Volumes and SUVRs had comparatively lower

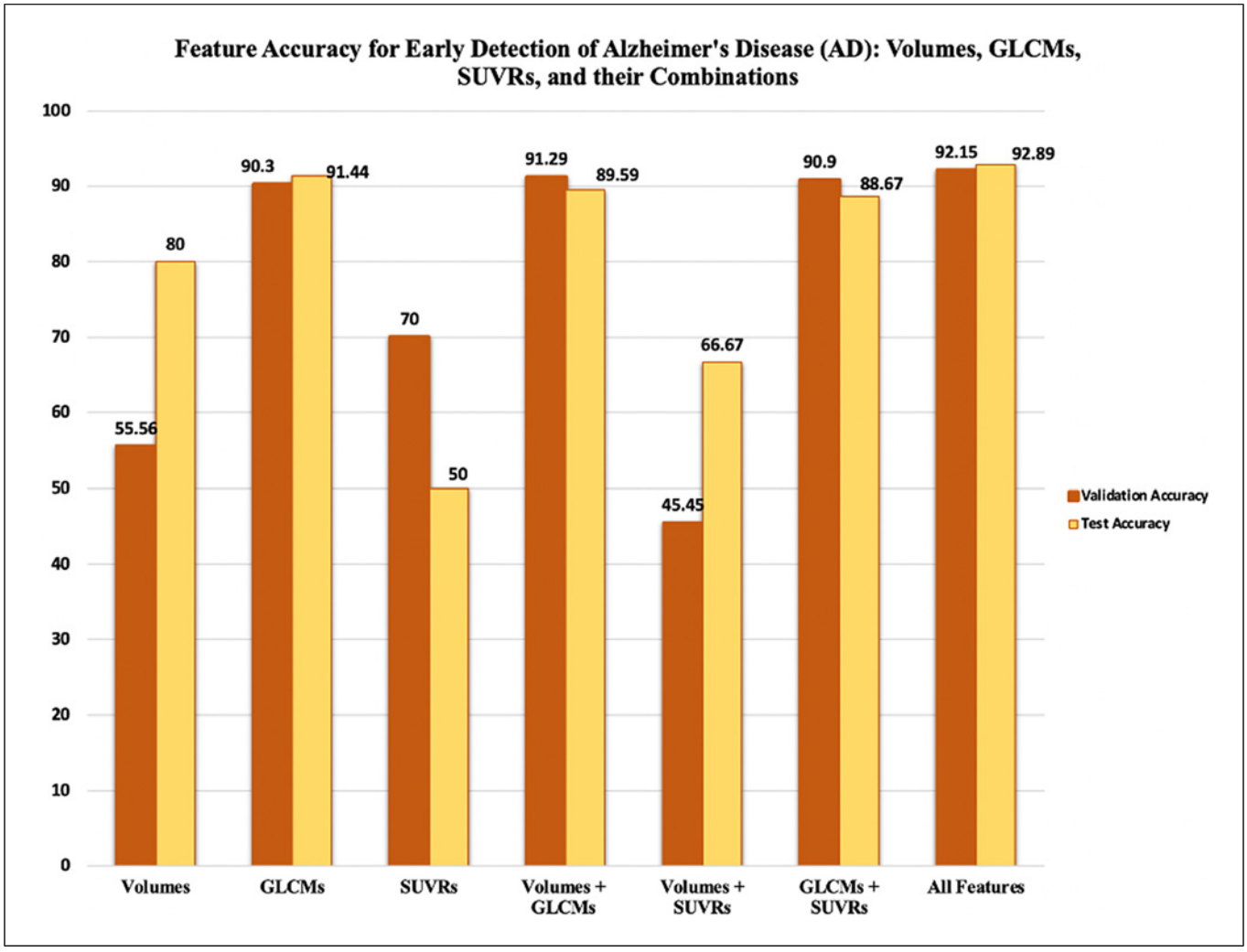

Fig. 10. Comparison of feature accuracy for early detection of Alzheimer's disease (AD): volumes, GLCMs, SUVRs, and their combinations.

performance when compared to GLCM texture features alone (shown in Fig. 10). Further analysis was done (see online suppl. material; for all online suppl. material, see https://doi.org/10.1159/00053886) to demonstrate that GLCM's features are more effective in differentiating between MCIc and MCIs.

Discussion

This study highlights the importance and discriminative ability of the texture features extracted from the hippocampus and entorhinal cortex in predicting MCI individuals who are prone to developing AD (MCIc) from those who will not (MCIs). This holds significant promise for clinical applications and the development of a digital biomarker model for early detection of AD. In other words, the integration of texture features into diagnostic protocols could provide clinicians with objective measures for accurate tracking of disease progression and aiding in therapeutic decision-making. As well as helping them in establishing more precise prognoses for patients diagnosed with MCIc, thus enabling timely interventions and personalized patient care strategies. Moreover, the lower false-positive rates associated with GLCM classifications offer a potential tool to minimize misdiagnoses, reducing unnecessary stress and treatment for patients who may not develop AD (MCIs). Moreover, it performs well and has high sensitivity rates when it is fused with other features (volumes or SUVR). It signifies a potential

shift toward more accurate and earlier AD detection compared to volume and SUVR features and has the potential to significantly impact clinical practice.

While this study demonstrates the importance of texture features in predicting MCIc, further research and validation studies are needed to ensure that these textural features can properly be rendered into digital biomarkers, included in clinical protocols and routine clinical settings, with existing methodologies, and with the unique advantages of our proposed approach. Implementing our framework within a clinical setting involves not only the technical aspects of incorporating various data types but also the feasibility and scalability of the approach across different patient groups and imaging modalities, MRI, fMRI scans, and AD digital biomarkers. Addressing these differences is essential for an adaptable clinical framework deployment. Furthermore, our study not only goes beyond the scope of existing methodologies, exemplified by the work of [46], and focuses on the main regions that are affected by AD at the onset, but also presents an innovative integration model. This integration encompasses machine learning, feature engineering, feature fusion, and feature importance analysis, emphasizing the distinctive benefits of our contribution. Moreover, the features analyzed in our study are different from those in their investigation. We included the SUVR which is associated with an increased risk of developing neurodegenerative diseases such as Alzheimer's. This work puts forth our findings in the landscape of AD feature importance analysis through machine learning models.

Conclusion

This study established a framework for the early detection of AD by classifying fused feature vectors from the hippocampus and entorhinal cortex 2D-GLCM texture features and volume of 3DMRI, along with SUVR of PET images, into two primary yield classes – MCIs and MCIc. The importance of these features extracted from the hippocampus and entorhinal cortex was determined using four different classifiers: L-SVM, LDA, LR, and LRSGD classifier. The average and top-ranked importance of each feature were then calculated based on the output of those classifiers. The feature importance provides insights into the contribution of those different features in classifying the early stages of AD. Next, we proceeded to validate the significance of these feature importance findings by classifying various combinations of feature fusion vectors using a PNN classifier. This additional step allowed us to assess how well these importance rankings translated into predictive accuracy and confirmed the meaningfulness of our feature importance analysis.

The results of the study showed that GLCM texture features are significant important biomarkers for early detection of AD, and they perform better compared to the volume and SUVR features of the hippocampus and entorhinal cortex. This importance was verified through an evaluation of various feature combinations using the PNN classifier. The results demonstrated that certain feature-class fusion combinations exhibited higher on-target (sensitivity) rates. Notably, the fusion of GLCMs with other features (volume or SUVR) yielded an impressive sensitivity (approximately 90% and higher), highlighting its effectiveness in accurately identifying MCIc cases. Additionally, GLCMs showed relatively lower false-positive rates for MCIs and MCIc cases (less than 30%), compared to SUVRs and volumes which have higher false-positive rates, indicating a higher chance of false-positive identifications for these groups. Moreover, the receiver operating characteristic curves for GLCMs and their fusions exhibited discriminatory ability in distinguishing between MCIs and MCIc classes compared to volume and SUVRs, indicating a poorer performance for this particular fusion. Furthermore, the study's results emphasize that fusing different types of features can lead to better classification performance and informative more than using any category of features alone.

In summary, our study distinguishes itself from reported work in the literature because it is focused on the classification of MCIs and MCIc, a distinctive patient group not yet extensively explored. Moreover, in this work, we implemented a novel feature engineering scheme and standardized all texture features (GLCM texture features, volume, and SUVR) from both the hippocampus and entorhinal cortex regions. These unique aspects of our research deepen the understanding of the significance of each feature in the classification of MCIs and MCIc patients, which ranks features from most to least significant. This provides a distinctive viewpoint on each feature's role in cognitive impairment and improves our knowledge of the effects of those features on the classification of AD patients. For future work, it may be beneficial to explore additional affected brain regions beyond the hippocampus and entorhinal cortex to further improve the proposed framework. Additionally, investigating more features such as surface area, cortical thickness, and folding index could improve our understanding of the significant features that help in detecting AD early-onset symptoms.

Acknowledgments

We would like to acknowledge that data used in the preparation of this article were obtained from the Alzheimer's Disease Neuroimaging Initiative (ADNI) database (www.loni.ucla.edu/ADNI). As such, the investigators within ADNI contributed to the design and implementation of ADNI and/or provided data but did not participate in the analysis or writing of this report. A complete listing of ADNI investigators is available at www.loni.ucla.edu/ADNI/Collaboration/ADNI_Manuscript_Citations.pdf. In addition, this work was supported by funds from the Faculty Research and Creative Activities Award at Western Michigan University.

Statement of Ethics

The Western Michigan University Institutional Review Board (IRB) granted this project exempt status.

Conflict of Interest Statement

The authors have no conflicts of interest to declare.

Funding Sources

This work was supported by funds from the Faculty Research and Creative Activities Award at Western Michigan University.

Author Contributions

Aya Hassouneh: literature review, conceptualization, research method implementation, experimental work setup and implementation, manuscript writing, leading the effort, and project administration. Bradley Bazuin and Alessander Danna-dos-Santos: conceptualization, discussion, reviewing, and editing. Ilgin Acar: reviewing. Ikhlas Abdel-Qader: conceptualization, research methods, experimental work setup, discussion, reviewing, editing, and project supervision.

Data Availability Statement

The data used in this study cannot be publicly disclosed due to the ADNI Data Use Agreement Policy. However, interested parties may obtain it through the Alzheimer's Disease Neuroimaging Initiative (ADNI) database (adni.loni.usc.edu).

References

1 SellesOliveira MCMM, Ferreira STMM, Ferreira ST. Brain inflammation connects cognitive and non-cognitive symptoms in Alzheimer's disease. J Alzheimers Dis. 2018;64:S313–27. doi: 10.3233/JAD-179925.
2 DeKosky ST, Marek K. Looking backward to move forward: early detection of neurodegenerative disorders. Science. 2003;302(5646):830–4. doi: 10.1126/science.1090349.
3 Fan Y, Batmanghelich N, Clark CM, Davatzikos C, Alzheimer's Disease Neuroimaging Initiative. Spatial patterns of brain atrophy in MCI patients, identified via high-dimensional pattern classification, predict subsequent cognitive decline. Neuroimage. 2008;39(4):1731–43. doi: 10.1016/j.neuroimage.2007.10.031.
4 Wang P, Chen K, Yao L, Hu B, Wu X, Zhang J, et al. Multimodal classification of mild cognitive impairment based on partial least squares. J Alzheimers Dis. 2016;54(1):359–71. doi: 10.3233/JAD-160102.
5 Zhang D, Wang Y, Zhou L, Yuan H, Shen D, Initiative ADN. Multimodal classification of Alzheimer's disease and mild cognitive impairment. Neuroimage. 2011;55(3):856–67. doi: 10.1016/j.neuroimage.2011.01.008.
6 Gupta Y, Kim J-I, Kim BC, Kwon G-R. Classification and graphical analysis of Alzheimer's disease and its prodromal stage using multimodal features from structural, diffusion, and functional neuroimaging data and the APOE genotype. Front Aging Neurosci. 2020;12:238. doi: 10.3389/fnagi.2020.00238.
7 DeAngelis LM. Brain tumors. N Engl J Med Overseas Ed. 2001;344(2):114–23. doi: 10.1056/nejm200101113440207.
8 Bauer S, Wiest R, Nolte LP, Reyes M. A survey of MRI-based medical image analysis for brain tumor studies. Phys Med Biol. 2013;58(13):R97–129. doi: 10.1088/0031-9155/58/13/R97.
9 Jones G, Wright J, Regele O, Kourtis L, Pszenny S, Sirkar R, et al. Evolution of the digital biomarker ecosystem. Digit Med. 2017;3(4):154–63. doi: 10.4103/digm.digm_35_17.
10 Tröger J, Baykara E, Zhao J, ter Huurne D, Possemis N, Mallick E, et al. Validation of the remote automated ki: e speech biomarker for cognition in mild cognitive impairment: verification and validation following DiME V3 Framework. Digit Biomark. 2022;6(3):107–16. doi: 10.1159/000526471.
11 Braak H, Braak E. Neuropathological stageing of Alzheimer-related changes. Acta Neuropathol. 1991;82(4):239–59. doi: 10.1007/BF00308809.
12 Ahmad F, Zulifqar H, Malik T. Classification of Alzheimer disease among susceptible brain regions. Int J Imaging Syst Technol. 2019;29(3):222–33. doi: 10.1002/ima.22308.
13 Xia H, Tong L, Zhou X, Zhang J, Zhou Z, Liu W. Texture analysis and volumetry of hippocampus and medial temporal lobe in patients with alzheimer's disease. International Conference on Biomedical Engineering and Biotechnology, IEEE; 2012. p. 905–8.
14 Acharya UR, Fernandes SL, WeiKoh JE, Ciaccio EJ, Fabell MKM, Tanik UJ, et al. Automated detection of Alzheimer's disease using brain MRI images–a study with various feature extraction techniques. J Med Syst. 2019;43(9):302–14. doi: 10.1007/s10916-019-1428-9.
15 Akhila DB, Shobhana S, Fred AL, Kumar SN. Robust Alzheimer's disease classification based on multimodal neuroimaging. IEEE international conference on engineering and technology (ICETECH), IEEE; 2016. p. 748–52.
16 Prakash K, Saradha S. Efficient prediction and classification for cirrhosis disease using LBP, GLCM and SVM from MRI images. Mater Today Proc. 2021.
17 Terada T, Therriault J, Kang MSP, Savard M, Pascoal TA, Lussier F, et al. Mitochondrial complex I abnormalities is associated with tau and clinical symptoms in mild Alzheimer's disease. Mol Neurodegener. 2021;16(1):28–12. doi: 10.1186/s13024-021-00448-1.
18 Iaccarino L, Tammewar G, Ayakta N, Baker SL, Bejanin A, Boxer AL, et al. Local and distant relationships between amyloid, tau and neurodegeneration in Alzheimer's Disease. Neuroimage Clin. 2018;17:452–64. doi: 10.1016/j.nicl.2017.09.016.
19 Mueller SG, Weiner MW, Thal LJ, Petersen RC, Jack CR, Jagust W, et al. Ways toward an early diagnosis in alzheimer's disease: the alzheimer's disease neuroimaging initiative (ADNI). Alzheimer's Dementia. 2005;1(1):55–66. doi: 10.1016/j.jalz.2005.06.003.

20 Patenaude B, Smith SM, Kennedy DN, Jenkinson M. A Bayesian model of shape and appearance for subcortical brain segmentation. Neuroimage. 2011;56(3):907–22. doi: 10.1016/j.neuroimage.2011.02.046.
21 Insausti R, Muñoz-López M, Insausti AM, Artacho-Pérula E. The human periallocortex: layer pattern in presubiculum, parasubiculum and entorhinal cortex. A review. Front Neuroanat. 2017;11:84. doi: 10.3389/fnana.2017.00084.
22 Bernasconi N, Bernasconi A, Andermann F, Dubeau F, Feindel W, Reutens DC. Entorhinal cortex in temporal lobe epilepsy: a quantitative MRI study. Neurology. 1999;52(9):1870–6. doi: 10.1212/wnl.52.9.1870.
23 Woolrich MW, Jbabdi S, Patenaude B, Chappell M, Makni S, Behrens T, et al. Bayesian analysis of neuroimaging data in FSL. Neuroimage. 2009;45(1 Suppl l):S173–86. doi: 10.1016/j.neuroimage.2008.10.055.
24 Jenkinson M, Beckmann CF, Behrens TEJ, Woolrich MW, Smith SM. Fsl. Neuroimage. 2012;62(2):782–90. doi: 10.1016/j.neuroimage.2011.09.015.
25 Turski WA, Cavalheiro EA, Bortolotto ZA, Mello LM, Schwarz M, Turski L. Seizures produced by pilocarpine in mice: a behavioral, electroencephalographic and morphological analysis. Brain Res. 1984;321(2):237–53. doi: 10.1016/0006-8993(84)90177-x.
26 Liu Z, Lu H, Pan X, Xu M, Lan R, Luo X. Diagnosis of Alzheimer's disease via an attention-based multi-scale convolutional neural network. Knowl Based Syst. 2022;238:107942. doi: 10.1016/j.knosys.2021.107942.
27 Terni B, Boada J, Portero-Otin M, Pamplona R, Ferrer I. Mitochondrial ATP-synthase in the entorhinal cortex is a target of oxidative stress at stages I/II of Alzheimer's disease pathology. Brain Pathol. 2010;20(1):222–33. doi: 10.1111/j.1750-3639.2009.00266.x.
28 Sudharsan M, Thailambal G. Alzheimer's disease prediction using machine learning techniques and principal component analysis (PCA). Mater Today Proc. 2021.
29 Horie K, Salvadó G, Barthélemy NR, Janelidze S, Li Y, He Y, et al. CSF MTBR-tau243 is a specific biomarker of tau tangle pathology in Alzheimer's disease. Nat Med. 2023;29(8):1954–63. doi: 10.1038/s41591-023-02443-z.
30 Gad AF, Gad AF, John S. Practical computer vision applications using deep learning with CNNs. Springer; 2018.
31 Mohanaiah P, Sathyanarayana P, GuruKumar L. Image texture feature extraction using GLCM approach. Int J scientific Res publications. 2013;3(5):1–5.
32 Sathiyamoorthi V, Ilavarasi AK, Murugeswari K, Thouheed Ahmed S, Aruna Devi B, Kalipindi M. A deep convolutional neural network based computer aided diagnosis system for the prediction of Alzheimer's disease in MRI images. Measurement. 2021;171:108838. doi: 10.1016/j.measurement.2020.108838.
33 Zheng A, Casari A. Feature engineering for machine learning: principles and techniques for data scientists. O'Reilly Media, Inc; 2018.
34 Zdravevski E, Lameski P, Mingov R, Kulakov A, Gjorgjevikj D. Robust histogram-based feature engineering of time series data. federated conference on computer science and information systems (FedCSIS) IEEE; 2015. p. 381–8.
35 Gupta Y, Lama RK, Lee S-W, Kwon G-R. An MRI brain disease classification system using PDFB-CT and GLCM with kernel-SVM for medical decision support. Multimed Tools Appl. 2020;79(43–44):32195–224. doi: 10.1007/s11042-020-09676-x.
36 Liu Z, Lu H, Pan X, Xu M, Lan R, Luo X. Diagnosis of Alzheimer's disease via an attention-based multi-scale convolutional neural network. Knowl Based Syst. 2022;238:107942. doi: 10.1016/j.knosys.2021.107942.
37 Seshadri S, Fitzpatrick AL, Ikram MA, DeStefano AL, Gudnason V, Boada M, et al. Genome-wide analysis of genetic loci associated with Alzheimer disease. JAMA. 2010;303(18):1832–40. doi: 10.1001/jama.2010.574.
38 Wang D, Wang P, Bian X, Xu S, Zhou Q, Zhang Y, et al. Elevated plasma levels of exosomal BACE1-AS combined with the volume and thickness of the right entorhinal cortex may serve as a biomarker for the detection of Alzheimer's disease. Mol Med Rep. 2020;22(1):227–38. doi: 10.3892/mmr.2020.11118.
39 Harris CR, Millman KJ, van der Walt SJ, Gommers R, Virtanen P, Cournapeau D, et al. Array programming with NumPy. Nature. 2020;585(7825):357–62. doi: 10.1038/s41586-020-2649-2.
40 Okamura N, Harada R, Furumoto S, Arai H, Yanai K, Kudo Y. Tau PET imaging in Alzheimer's disease. Curr Neurol Neurosci Rep. 2014;14:1–7.
41 Barthélemy NR, Horie K, Sato C, Bateman RJ. Blood plasma phosphorylated-tau isoforms track CNS change in Alzheimer's disease. J Exp Med. 2020;217(11):e20200861. doi: 10.1084/jem.20200861.
42 Vemuri P, Lowe VJ, Knopman DS, Senjem ML, Kemp BJ, Schwarz CG, et al. Tau-PET uptake: regional variation in average SUVR and impact of amyloid deposition. Alzheimers Dement. 2017;6:21–30. doi: 10.1016/j.dadm.2016.12.010.
43 Shen D, Wee C-Y, Zhang D, Zhou L, Yap P-T. Machine learning techniques for AD/MCI diagnosis and prognosis. Machine learning in healthcare informatics Springer; 2014. p. 147–79.
44 Asim Y, Raza B, Malik AK, Rathore S, Hussain L, Iftikhar MA. A multi-modal, multi-atlas-based approach for Alzheimer detection via machine learning. Int J Imaging Syst Technol. 2018;28(2):113–23. doi: 10.1002/ima.22263.
45 Balne S, Elumalai A. Machine learning and deep learning algorithms used to diagnosis of Alzheimer's: review. Mater Today Proc. 2021;47:5151–6. doi: 10.1016/j.matpr.2021.05.499.
46 Diogo VS, Ferreira HA, Prata D, Alzheimer's Disease Neuroimaging Initiative. Early diagnosis of Alzheimer's disease using machine learning: a multi-diagnostic, generalizable approach. Alzheimers Res Ther. 2022;14(1):107. doi: 10.1186/s13195-022-01047-y.
47 Cortes C, Vapnik V. Support-vector networks. Mach Learn. 1995;20(3):273–97. doi: 10.1007/bf00994018.
48 Balakrishnama S, Ganapathiraju A. Linear discriminant analysis-a brief tutorial. Inst Signal Inf Process. 1998;18:1–8.
49 Hosmer DW Jr, Lemeshow S, Sturdivant RX. Applied logistic regression. John Wiley & Sons; 2013. Vol. 398.
50 Bottou L. Large-scale machine learning with stochastic gradient descent. Proceedings of COMPSTAT'2010: 19th International conference on computational StatisticsParis France, august 22-27, 2010 keynote, invited and contributed papers Springer; 2010. p. 177–86.
51 Mathew NA, Vivek RS, Anurenjan PR. Early diagnosis of Alzheimer's disease from MRI images using PNN. International CET conference on control, communication, and computing (IC4) IEEE; 2018. p. 161–4.
52 Hassouneh A, Bazuin B, Kaku H, Abdel-Qader I. A data fusion framework for mild cognitive impairment classification: hippocampal volume and GLCM features using machine learning. ICITA. 2023.
53 Specht DF. Probabilistic neural networks. Neural networks. 1990;3(1):109–18. doi: 10.1016/0893-6080(90)90049-q.
54 Sørensen L, Igel C, Liv Hansen N, Osler M, Lauritzen M, Rostrup E, et al. Early detection of Alzheimer's disease using M RI hippocampal texture. Hum Brain Mapp. 2016;37(3):1148–61. doi: 10.1002/hbm.23091.
55 Leandrou S, Lamnisos D, Mamais I, Kyriacou PA, Pattichis CS, Alzheimer's Disease and Neuroimaging Initiative. Assessment of Alzheimer's disease based on texture analysis of the entorhinal cortex. Front Aging Neurosci. 2020;12:176. doi: 10.3389/fnagi.2020.00176.
56 Castellano G, Bonilha L, Li LM, Cendes F. Texture analysis of medical images. Clin Radiol. 2004;59(12):1061–9. doi: 10.1016/j.crad.2004.07.008.